



## A Unified Distributed Control Strategy for Hybrid Cascaded-Parallel Microgrid

Yuan, Wenbin; Wang, Yanbo; Ge, Xiaohai; Hou, Xiaochao; Han, Hua

*Published in:*  
IEEE Transactions on Energy Conversion

*DOI (link to publication from Publisher):*  
[10.1109/TEC.2019.2931886](https://doi.org/10.1109/TEC.2019.2931886)

*Publication date:*  
2019

*Document Version*  
Accepted author manuscript, peer reviewed version

[Link to publication from Aalborg University](#)

*Citation for published version (APA):*  
Yuan, W., Wang, Y., Ge, X., Hou, X., & Han, H. (2019). A Unified Distributed Control Strategy for Hybrid Cascaded-Parallel Microgrid. *IEEE Transactions on Energy Conversion*, 34(4), 2029-2040. Article 8781936. <https://doi.org/10.1109/TEC.2019.2931886>

### General rights

Copyright and moral rights for the publications made accessible in the public portal are retained by the authors and/or other copyright owners and it is a condition of accessing publications that users recognise and abide by the legal requirements associated with these rights.

- Users may download and print one copy of any publication from the public portal for the purpose of private study or research.
- You may not further distribute the material or use it for any profit-making activity or commercial gain
- You may freely distribute the URL identifying the publication in the public portal -

### Take down policy

If you believe that this document breaches copyright please contact us at [vbn@aub.aau.dk](mailto:vbn@aub.aau.dk) providing details, and we will remove access to the work immediately and investigate your claim.

# A Unified Distributed Control Strategy for Hybrid Cascaded-Parallel Microgrid

Wenbin Yuan, Yanbo Wang, *Member, IEEE*, Xiaohai Ge, Xiaochao Hou, and Hua Han

**Abstract**— Hybrid cascaded-parallel microgrid is becoming a new emerging structure to integrate multiple low-voltage power sources. This paper presents a unified distributed control strategy to implement power sharing control in hybrid cascaded-parallel microgrid under both resistive-inductive (RL) and resistive-capacitive (RC) load, where a sign function is introduced to automatically match load characteristic. Active power and reactive power regulators without frequency drop are developed, and low bandwidth communication network is employed to support power management and improve system redundancy. Furthermore, small signal model of hybrid cascaded-parallel microgrid with RL load and RC load is established. Also, small signal stability and dynamic performance of the proposed distributed control strategy is investigated. Simulation results show that the unified distributed control strategy is able to implement desirable power sharing under different load types with superior control performance. Also, the proposed control strategy is able to improve system redundancy and support plug-and-play operation of microgrid.

**Index Terms**—Hybrid cascaded-parallel microgrid, distributed control, power sharing, low band width communication.

## I. INTRODUCTION

MICROGRID is becoming an attractive and promising structure to integrate renewable energies into power system [1]-[2], which can enhance reliability and flexibility of power supply. Autonomous microgrids can be typically classified as parallel-type [3] and cascaded-type [4] as shown in Fig.1(a)-(b). Recently, hybrid cascaded-parallel microgrid is proposed as a promising structure [5]-[6] to support high power operation as shown in Fig.1(c), which can be applied for low-voltage (LV) power sources integrating such as cascaded PV panels and battery cells. However, power control strategy of hybrid cascaded-parallel microgrid has merely been concerned.

In parallel-type microgrids, power control issue is one of important concerns in autonomous microgrids. Droop control strategies have been frequently developed to perform proportional power assignment in parallel-type microgrids [7]-[8]. However, implementation of droop control tends to cause an undesirable frequency deviation, which thus weakens

power quality. Currently, no single decentralized control can guarantee frequency/voltage regulation and exact active/reactive power sharing at the same time [9]. Thus, communication-based control methods have been widely researched. The centralized control is presented in [10]-[11]. By installing current sharing module to broadcast current reference to each inverter, the current sharing is maintained during both steady state and transients. However, these methods need high-bandwidth communication links between central controller and each inverter, which reduces the system reliability and may impose single point of failure on the central controller [12]. Moreover, the plug-and-play feature is not available since the central controller needs to reset parameters when a new DG is added to the system. Also, distributed control method has been paid much attention due to redundancy and scalability. In distributed control, each DG unit exchanges information with others according to defined communication protocols [13]-[15], where only low-bandwidth communication (LBC) network is required to implement synchronization operation among all inverters. In addition, single point of failure can be avoided in distributed control by properly designing communication network, enhancing system reliability and redundancy [16]-[17].

The cascaded-type microgrid is also proposed for high power application [18]-[25] as shown in Fig.1(b). Especially, this topology is practical for integrating LV photovoltaic sources into medium-voltage (MV) power system using LV devices [18]-[19]. Similarly, most power sharing methods of cascaded-type system are centralized with high-bandwidth communication [18]-[21], which mitigates system reliability and flexibility. An inverse droop control strategy is proposed in [22] to perform power sharing without using communication links. However, this method is only applicable for microgrid with resistive-inductive (RL) load. To overcome this limitation, [23] proposes a frequency-active power/reactive power ( $f$ - $P/Q$ ) droop control strategy to perform power sharing for microgrid with RL load and resistive-capacitive (RC) load. Considering diverse user demands, a unified droop control is proposed in [24] to enhance stable operation under four-quadrant modes. [25] has introduced a  $P$ - $\omega$  droop control for the grid-connected cascaded inverters. The necessary and sufficient condition of system stability is also presented. However, methods in [18]-[25] cannot perform unified power control in hybrid cascaded-parallel microgrid, which is addressed in this paper.

Hybrid cascaded-parallel microgrid structure as shown in Fig.1(c) is proposed in [5]-[6] for high power application,

W. Yuan, and Y. Wang are with the Department of Energy Technology, Aalborg University, Aalborg 9220, Denmark (e-mail: wyu@et.aau.dk; ywa@et.aau.dk).

X. Ge, X. Hou, and H. Han are with the School of Automation, Central South University, Changsha 410083, China (e-mail: gexiaohai@csu.edu.cn; houxc10@csu.edu.cn; hua\_han@126.com).

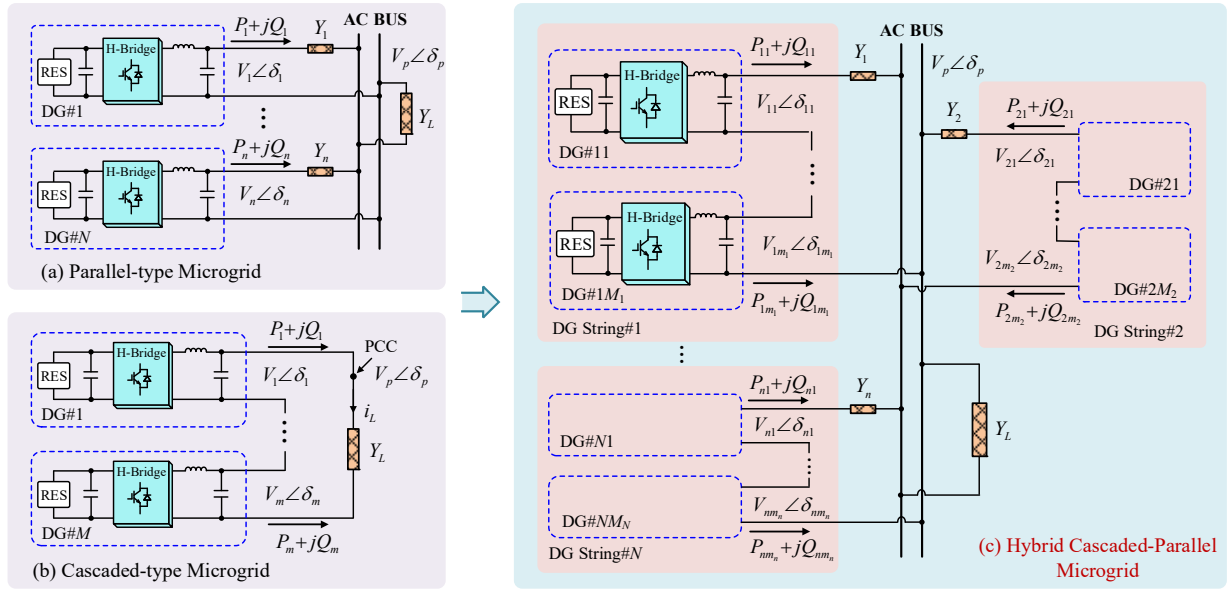


Fig. 1. Architectures of microgrid. (a) Parallel-type microgrid. (b) Cascaded-type microgrid. (c) Hybrid cascaded-parallel microgrid.

which is able to provide high flexibility and reduce operation cost. However, power control strategy in cascaded-parallel microgrid with both RL and RC load is slightly developed. A hierarchical control structure is developed in [5] to perform power sharing and synchronization operation, where centralized control method is implemented to distribute the power demand among cascaded inverters. However, the application of central controllers weakens reliability and flexibility of paralleled strings. Communication-less power control strategy for cascaded-parallel microgrid is slightly developed.

Therefore, this paper presents a unified distributed control method. The main contributions in this work are explained as follows. (1) A unified distributed control strategy is proposed to implement power control under both RL and RC load. (2) Small signal stability and dynamic performance of hybrid microgrid with the proposed distributed control strategy is investigated.

## II. POWER CONTROL CHARACTERISTIC OF PARALLEL-TYPE AND CASCADED-TYPE DROOP-CONTROLLED MICROGRIDS

In this section, power control characteristic of parallel-type and cascaded-type microgrids is analyzed.

### A. Power Control Characteristic of Parallel-type Microgrid

Fig.1(a) shows the circuit configuration of parallel-type microgrid. With the assumption of inductive feeder impedance, the output active power  $P_i$  and reactive power  $Q_i$  of the  $i$ -th DG are given as (1)-(2) [3],[24].

$$P_i = \frac{V_i V_p}{X_i} \sin(\delta_{iP}) \approx \frac{V_i V_p}{X_i} \delta_{iP} \quad (1)$$

$$Q_i = \frac{V_i (V_i - V_p)}{X_i} \quad (2)$$

where  $V_i$  is the output voltage amplitude of  $i$ -th inverter.  $V_p$  is the voltage amplitude of common AC bus.  $\delta_{iP}$  is the power angle difference between  $V_i$  and  $V_p$ .  $X_i$  is reactance of the feeder impedance between DG# $i$  and AC bus.

The relationship between  $\Delta P_i - \Delta \delta_i$  and  $\Delta Q_i - \Delta V_i$  can be simplified from (1)-(2) as (3)-(4).

$$\Delta P_i \propto \Delta \delta_i \quad (3)$$

$$\Delta Q_i \propto \Delta V_i \quad (4)$$

where  $\propto$  represents ‘‘a positive correlation’’.

The mathematical relationships (3)-(4) indicate that the output active and reactive power can be controlled by regulating frequency and voltage of inverters. Therefore, the conventional active power-angular frequency ( $P-\omega$ ) and reactive power-voltage ( $Q-V$ ) droop control can be given as (5)-(6) [26].

$$\omega_i = \omega^* - m_i P_i \quad (5)$$

$$V_i = V^* - n_i Q_i \quad (6)$$

where  $\omega_i$  is the angular frequency,  $\omega^*$  and  $V^*$  represent angular frequency and voltage amplitude without load.  $m_i$  and  $n_i$  are coefficients of  $P-\omega$  droop control and  $Q-V$  droop control, respectively.

### B. Power Control Characteristic of Cascaded-type Microgrid

Since power control characteristic in cascaded-type microgrid is different with that in parallel-type microgrid, an  $f-P/Q$  droop control is introduced in [23] to perform power control among cascaded inverters, whose principle is revealed as follows.

In the cascaded-type microgrid shown in Fig. 1(b), output power of the  $i$ -th DG is given as (7)-(8) [23].

$$P_i = V_i |Y_L| \sum_{j=1}^n V_j \cos(\delta_{ij} - \varphi_L) \quad (7)$$

$$Q_i = V_i |Y_L| \sum_{j=1}^n V_j \sin(\delta_{ij} - \varphi_L) \quad (8)$$

where  $|Y_L|$  and  $\varphi_L$  are the amplitude and angle of load admittance.  $\delta_{ij}$  is the power angle between DG# $i$  and DG# $j$ , which is much smaller than  $\varphi_L$  in steady state. Then,  $\Delta P_i - \Delta \delta_i$  and  $\Delta Q_i - \Delta V_i$  relationships are given as (9) and (10).

$$\Delta P_i \propto \sin(\varphi_L) \Delta \delta_i \quad (9)$$

$$\Delta Q_i \propto -\sin(\varphi_L) \Delta V_i \quad (10)$$

Fig. 2 and Fig. 3 show the  $\Delta P_i - \Delta \delta_i$  and  $\Delta Q_i - \Delta V_i$  relationships in cascaded-type microgrid. With RL load, there is  $\sin(\varphi_L) < 0$ , which means the  $\Delta P_i$  has a negative correlation with  $\Delta \delta_i$  and  $\Delta Q_i$  has a positive correlation with  $\Delta V_i$ . In this case, the  $P$ - $\omega$  inverse droop control and conventional  $Q$ - $V$  droop control should be adopted. With RC load,  $\Delta P_i$  has a positive correlation with  $\Delta \delta_i$  and  $\Delta Q_i$  has a negative correlation with  $\Delta V_i$ , which means that the system can be stable under the conventional  $P$ - $\omega$  droop control and  $Q$ - $V$  inverse droop control.

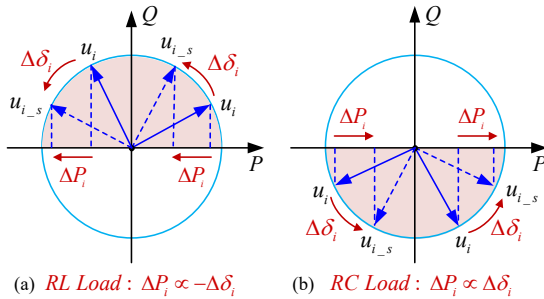


Fig. 2.  $\Delta P_i - \Delta \delta_i$  relationship in cascaded-type microgrid.

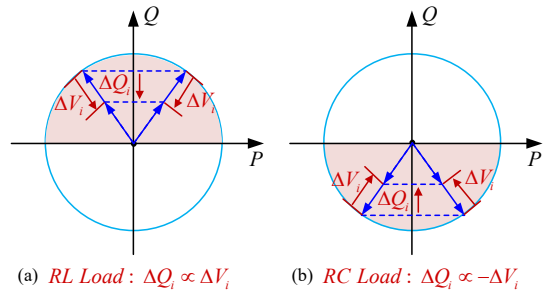


Fig. 3.  $\Delta Q_i - \Delta V_i$  relationship in cascaded-type microgrid.

TABLE I  
DECENTRALIZED POWER CONTROL OF MICROGRIDS

	Parallel-type Microgrid [26]		Cascaded-type Microgrid [23]	
	RL load	RC load	RL load	RC load
Power transmission characteristic	$\Delta P_i \propto \Delta \delta_i$	$\Delta P_i \propto \Delta \delta_i$	$\Delta P_i \propto -\Delta \delta_i$	$\Delta P_i \propto \Delta \delta_i$
	$\Delta Q_i \propto \Delta V_i$	$\Delta Q_i \propto \Delta V_i$	$\Delta Q_i \propto \Delta V_i$	$\Delta Q_i \propto -\Delta V_i$
Effective decentralized control	$\omega_i = \omega^* - m_i P_i$	$\omega_i = \omega^* - m_i P_i$	$\omega_i = \omega^* + m_i P_i$	$\omega_i = \omega^* - m_i P_i$
	$V_i = V^* - n_i Q_i$	$V_i = V^* - n_i Q_i$	$V_i = V^* - n_i Q_i$	$V_i = V^* + n_i Q_i$

The effective power control strategies of parallel- and cascaded-type microgrid with RL or RC load are summarized in Table I according to aforementioned analysis. It can be seen that neither droop control nor inverse droop control is compatible among cascaded and paralleled inverters under RL load or RC load, which means these decentralized control

methods are not applicable for hybrid cascaded-parallel microgrid. However, since the communication links are usually indispensable for fault monitoring and energy management, a distributed control strategy based on LBC thus can be designed to perform unified power control under RL load and RC load, which is presented in Section III.

### III. PROPOSED DISTRIBUTED CONTROL STRATEGY

In this section, a distributed control strategy is proposed to perform unified power control for hybrid cascaded-parallel microgrid with RL and RC load, which is able to implement proportional power sharing without frequency deviation.

#### A. Communication Network Design

Fig. 1(c) shows circuit configuration of the hybrid cascaded-parallel microgrid. Several LV DGs are cascaded-connected to provide a medium- or high-voltage. These cascaded DGs are then connected to AC bus in parallel to supply power to the load. Such a physical system can be equipped with a communication network to facilitate data exchange among DGs for control and monitoring purposes. Fig. 4 shows the graphical representation of communication network. In the graph, nodes represent DGs and edges connecting nodes represent communication links. Each node sends its active power and reactive power information to neighboring nodes. The information transmission can be bidirectional or unidirectional, and the graph is correspondingly called undigraph or digraph. In addition, nodes receive information from neighbors with different gains which are called communication weights. For example, if Node# $i$  receives data  $x_j$  from Node# $j$  with weight  $a_{ij}$ , it means that the information received by Node# $i$  is  $a_{ij} x_j$ . Usually,  $a_{ij} > 0$  if Node# $i$  receives information from Node# $j$  and  $a_{ij} = 0$ , otherwise. In the graph, an adjacency matrix  $A = [a_{ij}] \in \mathbb{R}^{N \times N}$  is defined to carry the communication weights. For each node, the weight in degree  $d_i^{in} = \sum_{j \in N_i} a_{ij}$  corresponds to the sum of weights of all ingoing edges into Node# $i$ , where  $N_i$  is the set of neighbors of Node# $i$ . The associated in-degree matrix is defined as  $D^{in} = \text{diag}\{d_i^{in}\}$ .

The Laplacian matrix is constructed as  $L = D^{in} - A$ .

In fact, for a system with a large number of DGs, topology of communication network may be various. However, there are some rules for managing a communication network. The mechanism can be explained as follows. Some definitions are first introduced. In the graph, a direct path from Node# $i$  to Node# $j$  is a sequence of edges connecting the two nodes. Root node is defined as a certain node, where there exists at least a direct path between the node and any other nodes. A graph includes a spanning tree if it contains a root node. A communication network is viewed as interconnection if it contains at least a spanning tree. Then, the rules of designing a communication network are given as follows [27]-[28]. (1) To ensure connectivity of communication tree, the network should contain at least one spanning tree. (2) To ensure system redundancy, the remaining communication network should still be connected in the case of any single communication link failure.

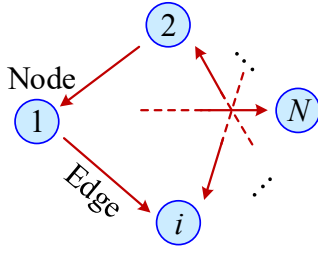


Fig. 4. Graphical representation of communication network.

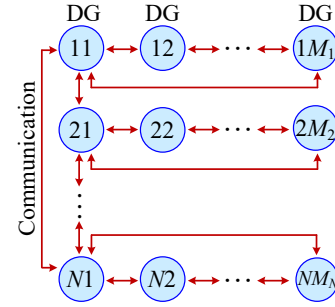


Fig. 5. Graphical diagram of the proposed communication network.

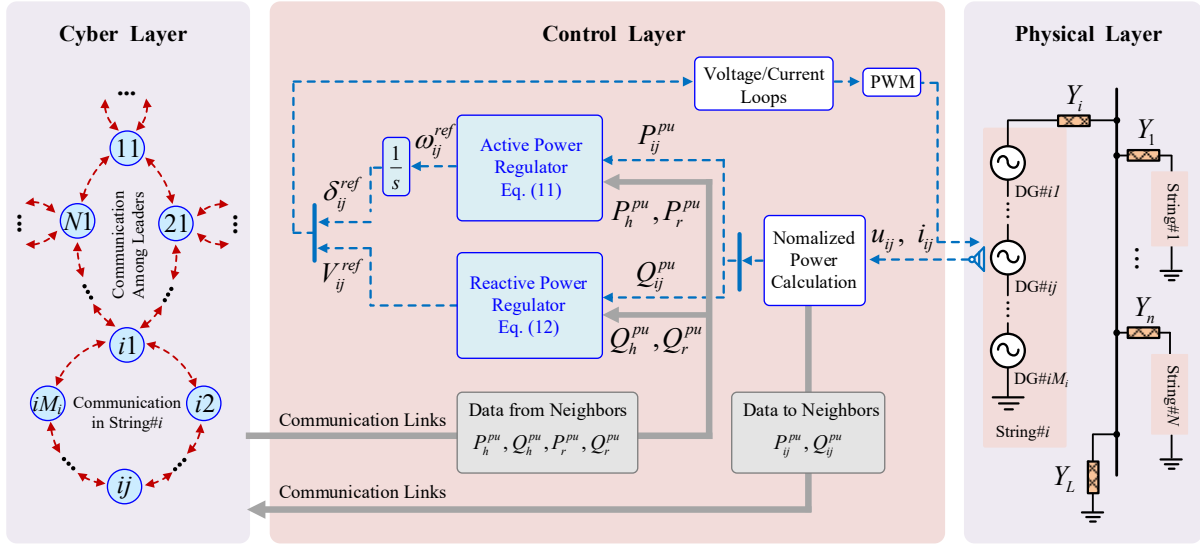


Fig. 6. Block diagram of proposed unified distributed control strategy.

In this paper, a bidirectional sparse-network with the minimum redundancy is developed. The graphical diagram of the proposed communication network is shown in Fig. 5. It has been proved that the ring structure is one of the most effective structures [28]. Here, the number  $ij$  ( $i=1, 2, \dots, N; j=1, 2, \dots, M_i$ ) denotes the  $j$ -th DG in the String $\#i$ , where  $N$  is the number of strings and  $M_i$  is the number of DGs in String $\#i$ . In the hybrid cascaded-parallel microgrid, information network includes communication links among cascaded DGs and those among paralleled DGs. Considering the sparsity, only one DG in each string is selected as a leader to exchange information with leaders of other strings. In addition, the mechanism for leader selection can be established for different objectives, and here we choose DGs with biggest rated power as leaders for optimum reliability.

### B. Proposed Unified Control Strategy of Hybrid Microgrid

In autonomous microgrids, the output power can be automatically assigned by controlling frequency and output voltage of DG unit. In hybrid microgrid, a distributed control strategy is proposed as (11)-(12).

$$\begin{aligned} \omega_{ij} &= \omega^* - \delta\omega_{ij}^1 + \delta\omega_{ij}^2 \\ \begin{cases} \delta\omega_{ij}^1 = \text{sgn}(Q_{ij}) k_{\omega}^{ij} \sum_{h \in N_{ij,s}} a_{ij,h} (P_h^{pu} - P_{ij}^{pu}) \\ \delta\omega_{ij}^2 = k_{\omega-p}^{ij} \sum_{r \in N_{ij,p}} a_{ij,r} (P_r^{pu} - P_{ij}^{pu}) \end{cases} & (11) \\ V_{ij} &= V_{ij}^* + \delta V_{ij}^1 + \delta V_{ij}^2 \\ \begin{cases} \delta V_{ij}^1 = \text{sgn}(Q_{ij}) \left( k_{V_p}^{ij} + \frac{k_{V_i}^{ij}}{s} \right) \sum_{h \in N_{ij,s}} a_{ij,h} (Q_h^{pu} - Q_{ij}^{pu}) \\ \delta V_{ij}^2 = \left( k_{V_p-p}^{ij} + \frac{k_{V_i-p}^{ij}}{s} \right) \sum_{r \in N_{ij,p}} a_{ij,r} (Q_r^{pu} - Q_{ij}^{pu}) \end{cases} & (12) \end{aligned}$$

where the subscript  $ij$  represents the  $j$ -th DG of string $\#i$ .  $h \in N_{ij,s}$  is the set of cascaded neighbors of DG $\#ij$ .  $r \in N_{ij,p}$  is the set of paralleled neighbors of DG $\#ij$ .  $a_{ij,h}$  ( $a_{ij,r}$ ) is the communication weight between DG $\#ij$  and DG $\#h$  (DG $\#r$ ), whose definition has been given in Section III.A.  $k_{\omega}^{ij}$  and  $k_{\omega-p}^{ij}$  are parameters of proportional controllers in the active power regulator (11).  $k_{V_p}^{ij}$ ,  $k_{V_i}^{ij}$ ,  $k_{V_p-p}^{ij}$  and  $k_{V_i-p}^{ij}$  are parameters of proportional-integral (PI) controllers in the reactive power regulator (12).  $P_{ij}^{pu}$  and  $Q_{ij}^{pu}$  are normalized active and reactive power of

DG# $ij$ , which are given as (13). The rated voltage amplitude  $V_{ij}^*$  is given as (14).

$$P_{ij}^{pu} = \frac{P_{ij}}{P_{ij}^{rated}}, \quad Q_{ij}^{pu} = \frac{Q_{ij}}{Q_{ij}^{rated}} \quad (13)$$

$$V_{ij}^* = \frac{Q_{ij}^{rated}}{\sum_{l=1}^{m_i} Q_{il}^{rated}} V_P^* \quad (14)$$

where  $P_{ij}^{rated}$  and  $Q_{ij}^{rated}$  are rated active and reactive power of DG# $ij$  and  $V_P^*$  is the rated voltage amplitude of AC bus.

Fig. 6 shows block diagram of the distributed control strategy. The distributed controller consists of active power regulator and reactive power regulator. Controller of DG# $ij$  receives information ( $P_{i'}^{pu}$ ,  $Q_{i'}^{pu}$ ,  $P_{i''}^{pu}$ ,  $Q_{i''}^{pu}$ ) from its neighbors and processes them with local data ( $P_{ij}^{pu}$ ,  $Q_{ij}^{pu}$ ) in two regulators. The frequency reference value is calculated by active power regulator according to (11). Here,  $\delta\omega_{ij}^1$  is added to mitigate the power mismatch among cascaded DGs, so a sign function  $\text{sgn}(Q_{ij})$  is introduced to match the different power transmission characteristics under RL load and RC load, ensuring the proposed controller effective under both situations. And  $\delta\omega_{ij}^2$  carries the active power mismatch between DG# $ij$  and its paralleled neighbors, which is zero for the non-leaders since the set  $N_{ij,p}$  is an empty set. The phase angle of DG# $ij$  is given as (15).

$$\delta_{ij} = \int \omega_{ij} dt = \omega^* t + \int \delta\omega_{ij}^1 dt + \int \delta\omega_{ij}^2 dt \quad (15)$$

It can be seen from (15) that the frequency of DG# $ij$  will synchronize to the rated value in the steady state. And  $\delta\omega_{ij}^1$  and  $\delta\omega_{ij}^2$  will converge to zero, which means accurate proportional active power sharing is guaranteed. In reactive power regulator, reactive power mismatch is fed to PI controllers, producing correction terms  $\delta V_{ij}^1$  and  $\delta V_{ij}^2$  to adjust the voltage amplitude. Similar with the active power regulator, a sign function  $\text{sgn}(Q_{ij})$  is introduced in  $\delta V_{ij}^1$  to match the different reactive power transmission characteristics under RL load and RC load. In the steady state,  $\delta V_{ij}^1$  and  $\delta V_{ij}^2$  decay to zero and all normalized reactive power synchronizes, which indicates the proportional reactive power sharing.

The proposed distributed control is a unified method for parallel and cascaded inverters under RL and RC load. Compared with central control method, DGs only need to exchange data with several neighbors by a low-bandwidth communication network. Therefore, single point of failure can be avoided so that the reliability and flexibility of microgrid can be enhanced.

#### IV. SMALL SIGNAL MODELING AND STABILITY ANALYSIS

Small signal stability of microgrids with proposed distributed control strategy is investigated in this section.

#### A. Small Signal Modeling

##### 1) Normalized power modeling

The power generation of the  $ij$ -th DG is presented as (16).

$$P_{ij} + jq_{ij} = \frac{V_{ij} e^{j\delta_{ij}}}{2} \left( \left( \sum_{b=1}^{m_i} V_{ib} e^{j\delta_{ib}} - V_P e^{j\delta_P} \right) |Y_i| e^{j\phi_i} \right)^* \quad (16)$$

where  $V_{ij}$  and  $\delta_{ij}$  represent the output voltage amplitude and phase angle of  $ij$ -th DG.  $V_P$  and  $\delta_P$  are the voltage amplitude and phase angle of AC bus.  $|Y_i|$  and  $\phi_i$  are the amplitude and angle of line admittance of String# $i$ . According to Kirchhoff laws, the voltage of AC bus is obtained as (17).

$$V_P e^{j\delta_P} = \sum_{a=1}^n \sum_{b=1}^{m_a} |Y_a'| V_{ab} e^{j\delta_{ab} + \phi_a'} \quad (17)$$

where

$$Y_a' = \frac{Y_a}{\sum_{c=1}^n Y_c + Y_L} = |Y_a'| e^{j\phi_a'} \quad (18)$$

Define  $\tilde{\delta}_{ij} = \delta_{ij} - \delta_s = \omega_{ij} - \omega_s$ , where  $\omega_s$  is the frequency in steady state. Then, combining (16)-(18), the instantaneous power supplied by the  $ij$ -th DG is given as (19).

$$\begin{cases} P_{ij} = \frac{1}{2} \sum_{a=1}^n \sum_{b=1}^{m_a} V_{ij} V_{ab} |Y_a'| |Y_i| \sin(\tilde{\delta}_{ij} - \tilde{\delta}_{ab} - \phi_a') - \frac{1}{2} \sum_{b=1}^{m_i} V_{ij} V_{ib} |Y_i| \sin(\tilde{\delta}_{ij} - \tilde{\delta}_{ib}) \\ = F(\tilde{\delta}_{11}, \tilde{\delta}_{12}, \dots, \tilde{\delta}_{nm_n}, V_{11}, V_{12}, \dots, V_{nm_n}) \\ q_{ij} = \frac{1}{2} \sum_{b=1}^{m_i} V_{ij} V_{ib} |Y_i| \cos(\tilde{\delta}_{ij} - \tilde{\delta}_{ib}) - \frac{1}{2} \sum_{a=1}^n \sum_{b=1}^{m_a} V_{ij} V_{ab} |Y_a'| |Y_i| \cos(\tilde{\delta}_{ij} - \tilde{\delta}_{ab} - \phi_a') \\ = G(\tilde{\delta}_{11}, \tilde{\delta}_{12}, \dots, \tilde{\delta}_{nm_n}, V_{11}, V_{12}, \dots, V_{nm_n}) \end{cases} \quad (19)$$

Instantaneous power is then passed through low-pass filter with the cutoff frequency  $\omega_c$ . The average active and reactive power are given as (20).

$$P_{ij} = \frac{\omega_c}{s + \omega_c} p_{ij}, \quad Q_{ij} = \frac{\omega_c}{s + \omega_c} q_{ij} \quad (20)$$

Combining (13), (19) and (20), small signal equations of normalized active and reactive power can be obtained as (21).

$$\begin{cases} \Delta \dot{P}^{pu} = \text{diag}\{-\omega_c\} \Delta P^{pu} + \omega_c K_{p^{pu}\tilde{\delta}} \Delta \tilde{\delta} + \omega_c K_{p^{pu}V} \Delta V \\ \Delta \dot{Q}^{pu} = \text{diag}\{-\omega_c\} \Delta Q^{pu} + \omega_c K_{q^{pu}\tilde{\delta}} \Delta \tilde{\delta} + \omega_c K_{q^{pu}V} \Delta V \end{cases} \quad (21)$$

where variable vectors ( $\Delta P^{pu}$ ,  $\Delta Q^{pu}$ ,  $\Delta \tilde{\delta}$  and  $\Delta V$ ) and parameter matrixes ( $K_{p^{pu}\tilde{\delta}}$ ,  $K_{p^{pu}V}$ ,  $K_{q^{pu}\tilde{\delta}}$  and  $K_{q^{pu}V}$ ) are given in Appendix.

##### 2) Distributed controller modeling

With the proposed distributed control, small signal models of active and reactive controllers are given as (22).

$$\begin{cases} \Delta \dot{\tilde{\delta}} = (K_\omega \text{diag}\{\text{sgn}(Q_{ij})\} L_s + K_{\omega-p} L_p) \Delta P^{pu} = K_1 \Delta P^{pu} \\ \Delta \dot{V} = (-K_p \text{diag}\{\text{sgn}(Q_{ij})\} L_s + K_{p-p} L_p) \Delta Q^{pu} \\ \quad + (-K_l \text{diag}\{\text{sgn}(Q_{ij})\} L_s + K_{l-p} L_p) \Delta Q^{pu} \\ = K_2 \Delta Q^{pu} + K_3 \Delta Q^{pu} \end{cases} \quad (22)$$

where  $K_\omega$ ,  $K_{\omega_p}$ ,  $K_P$ ,  $K_I$ ,  $K_{P_p}$ ,  $K_{I_p}$  are control coefficient matrixes.  $L_s$  and  $L_p$  are Laplacian matrixes carrying the information of cyber configuration. They are given in Appendix.

### 3) Overall small signal modeling

Small signal dynamic model of the whole system can be established by combining (21)-(22) as (23).

$$\Delta \dot{x} = A \Delta x \quad (23)$$

where

$$A = \begin{bmatrix} \Delta P^{pu} \Delta Q^{pu} \Delta \tilde{\delta} \Delta V \\ \text{diag}\{-\omega_c\} & 0_{m_n \times m_n} & \omega_c K_{p^{pu} \tilde{\delta}} & \omega_c K_{p^{pu} V} \\ 0_{m_n \times m_n} & \text{diag}\{-\omega_c\} & \omega_c K_{q^{pu} \tilde{\delta}} & \omega_c K_{q^{pu} V} \\ K_1 & 0_{m_n \times m_n} & 0_{m_n \times m_n} & 0_{m_n \times m_n} \\ 0_{m_n \times m_n} & \text{diag}\{\omega_c\} K_2 + K_3 & \omega_c K_{q^{pu} \tilde{\delta}} K_2 & \omega_c K_{q^{pu} V} K_2 \end{bmatrix} \quad (24)$$

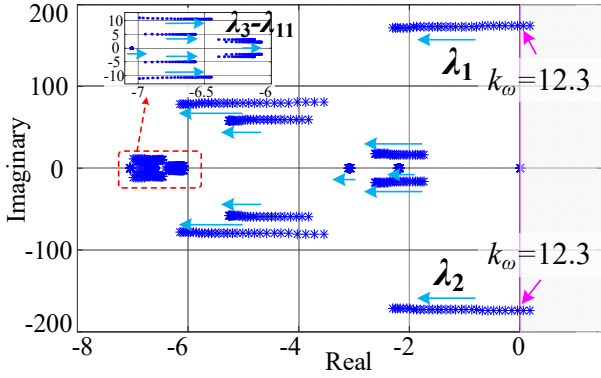


Fig. 7. Eigenvalue trajectory as  $k_\omega \in [0, 100]$ .

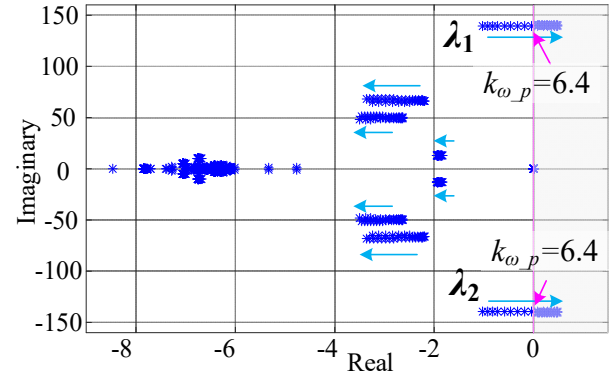


Fig. 8. Eigenvalue trajectory as  $k_{\omega_p} \in [0, 10]$ .

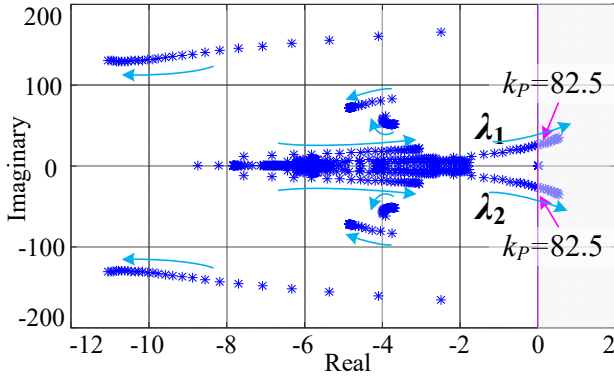


Fig. 9. Eigenvalue trajectory as  $k_P \in [0, 100]$ .

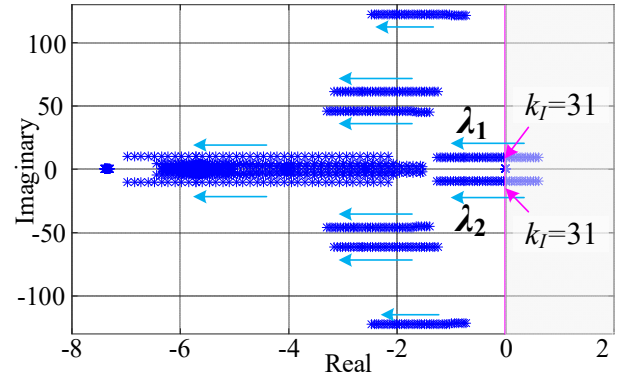


Fig. 10. Eigenvalue trajectory as  $k_I \in [0, 100]$ .

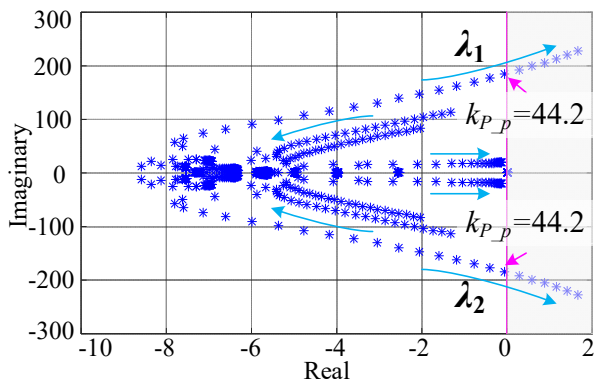


Fig. 11. Eigenvalue trajectory as  $k_{P_p} \in [0, 50]$ .

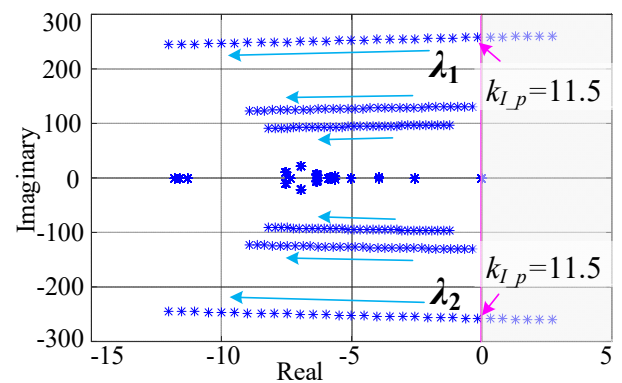


Fig. 12. Eigenvalue trajectory as  $k_{I_p} \in [0, 50]$ .

### B. Eigenvalue Analysis

The eigenvalues of matrix A can be calculated to investigate small signal stability of the system. According to the system parameters described in Section V, eigenvalue trajectory of system (23) is analyzed while varying the control parameters, where control parameters are identical for all DG units, defined as  $k_{\omega}$ ,  $k_{\omega_p}$ ,  $k_P$ ,  $k_I$ ,  $k_{P_p}$  and  $k_{I_p}$ . It is noted that matrix A has one zero eigenvalue which is corresponding to rotational symmetry and only the nonzero eigenvalues are valid for the system dynamic stability [29]-[31]. Since the system has similar response to the control parameters under RL and RC load, only the dynamic response under RL load is described, while the stability regions of control parameters under RC load can be found in Table II.

Fig. 7 and Fig. 8 show eigenvalue trajectories with  $k_{\omega}$  and  $k_{\omega_p}$  varying. In Fig. 7, when  $k_{\omega}$  is small, conjugate poles  $\lambda_1$  and  $\lambda_2$  are located in right half-plane, which means that system is unstable. The eigenvalue traces will move to left-half plane as increases of  $k_{\omega}$ . Meanwhile,  $\lambda_3 \sim \lambda_{11}$  move toward the imaginary axis decreasing the damping ratio of system. In Fig. 8, as  $k_{\omega_p}$  increases,  $\lambda_1$  and  $\lambda_2$  move toward unstable region and eventually lie on the right half-plane when  $k_{\omega_p}=6.4$ , making system unstable.

Fig. 9 and Fig. 10 show eigenvalue trajectories with  $k_P$  and  $k_I$  varying. It can be seen from Fig. 9 that increasing  $k_P$  attracts

the conjugate poles  $\lambda_1$  and  $\lambda_2$  to the imaginary axis, making the system unstable. It can also be seen from Fig. 10 that increasing  $k_I$  facilitates  $\lambda_1$  and  $\lambda_2$  moving away from the imaginary axis, keeping system stable. Parameters  $k_{P_p}$  and  $k_{I_p}$  have similar influence with  $k_P$  and  $k_I$  respectively, as shown in Fig. 11 and Fig. 12.

Fig. 7-12 show control parameters  $k_{\omega}$ ,  $k_{\omega_p}$ ,  $k_P$ ,  $k_I$ ,  $k_{P_p}$  and  $k_{I_p}$  have critical influence on system stability and dynamic performance. Taking the overshoot during transients into account, the stability regions of those parameters under RL load and RC load are shown in Table II.

TABLE II  
STABILITY REGION OF CONTROL PARAMETERS

RL Load		RC Load	
Parameter	Stability Region	Parameter	Stability Region
$k_{\omega}$	[12.3, 100]	$k_{\omega}$	[18, 100]
$k_{\omega_p}$	[0, 6.4]	$k_{\omega_p}$	[0, 5.3]
$k_P$	[0, 82.5]	$k_P$	[0, 76.2]
$k_I$	[31, 100]	$k_I$	[35.8, 100]
$k_{P_p}$	[0, 44.2]	$k_{P_p}$	[0, 39.5]
$k_{I_p}$	[11.5, 50]	$k_{I_p}$	[13.4, 50]

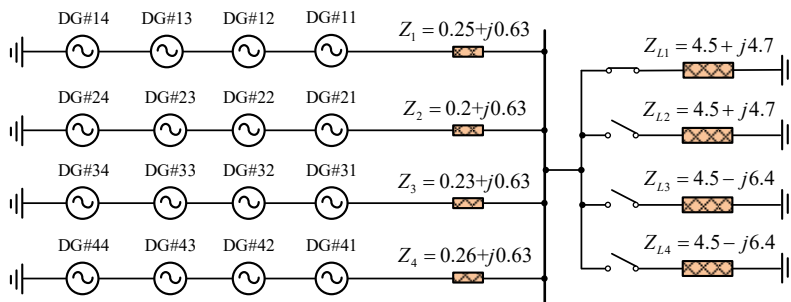


Fig. 13. Equivalent circuit of test microgrid.

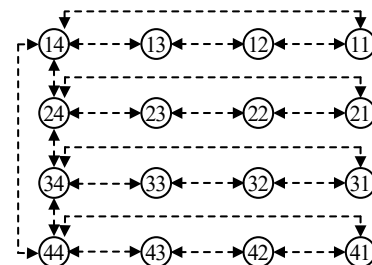


Fig. 14. Cyber configuration of test microgrid.

TABLE III  
SYSTEM PARAMETERS

Item	Value	Item	Value
Voltage amplitude reference of AC bus	$V_p^* = 311V$	Rated active power	$P_{11}^{rated} = P_{12}^{rated} = 1kW, P_{13}^{rated} = P_{14}^{rated} = 1.5kW$
Rated angular frequency	$\omega^* = 100\pi \text{ rad/s}$		$P_{21}^{rated} = P_{22}^{rated} = 2kW, P_{23}^{rated} = P_{24}^{rated} = 2.5kW$
Filter inductance	$L_f = 1.6 \text{ mH}$		$P_{31}^{rated} = P_{32}^{rated} = 3kW, P_{33}^{rated} = P_{34}^{rated} = 3.5kW$
Filter capacitance	$C_f = 20 \mu F$		$P_{41}^{rated} = P_{42}^{rated} = 4kW, P_{43}^{rated} = P_{44}^{rated} = 4.5kW$
Communication weights	$a_{ij_h, h \in N_{ij_s}} = 1, a_{ij_h, h \in N_{ij_p}} = 1$	Rated reactive power	$Q_{11}^{rated} = Q_{12}^{rated} = 1kVar, Q_{13}^{rated} = Q_{14}^{rated} = 1.5kVar$
Active power control coefficients	$k_{\omega} = 30, k_{\omega_p} = 3$		$Q_{21}^{rated} = Q_{22}^{rated} = 2kVar, Q_{23}^{rated} = Q_{24}^{rated} = 2.5kVar$
Reactive power control coefficients	$k_P = 35, k_I = 50$		$Q_{31}^{rated} = Q_{32}^{rated} = 3kVar, Q_{33}^{rated} = Q_{34}^{rated} = 3.5kVar$
	$k_{P_p} = 20, k_{I_p} = 30$		$Q_{41}^{rated} = Q_{42}^{rated} = 4kVar, Q_{43}^{rated} = Q_{44}^{rated} = 4.5kVar$

## V. SIMULATION RESULTS

To validate effectiveness of the proposed unified distributed control strategy, simulation verification is implemented in a scale-down AC microgrid with  $4 \times 4$  inverters in MATLAB. The circuit configuration of the exemplified microgrid is shown in Fig. 13. The ring communication network is shown in Fig. 14. The circuit and control parameters applied in simulation verification are given in Table III.

### A. Case I: Performance of Unified Distributed Controller

In this case, performance of proposed distributed control method is tested under RL load and RC load. In practical operation, there exist several trivial disturbances such as measurement noise and parameter perturbations [3], etc., which may deteriorate controller performance. Therefore, immunity capability to these disturbances is also tested in this case. Measurement noise is added to voltage/current measurement signals and stochastic disturbance is added to controller parameters. Fig. 15 shows simulation results under RL load. In order to analyze power sharing performance of proposed controller under different load profiles,  $Z_{L1}$  is connected at first and  $Z_{L2}$  is plugged at 2s. It can be seen from Fig. 15(a) that all inverter frequencies synchronize to the rated frequency of 50 Hz in the steady state without any deviation. And the system has a fast response with the load change. Fig. 15(b)-(c) show that proportional load sharing is accurately maintained among cascaded and paralleled sources. Fig. 16 shows simulation results under RC load, where  $Z_{L3}$  is connected at first and  $Z_{L4}$  is plugged at 2s. It can be seen that similar performance is achieved under RC load. These simulation results validate the effectiveness of unified power control strategy under RL and RC load. Furthermore, the proposed controller is able to deal with the effect of measurement noise and parameter perturbation as shown in Fig.15-16.

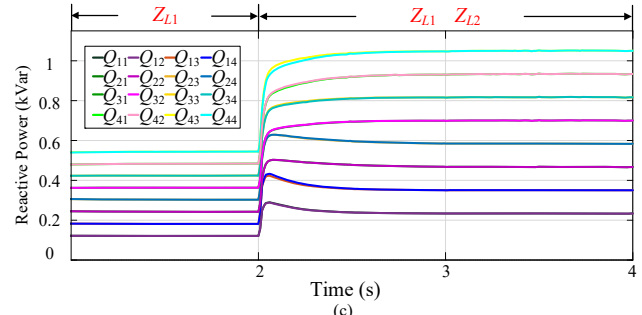
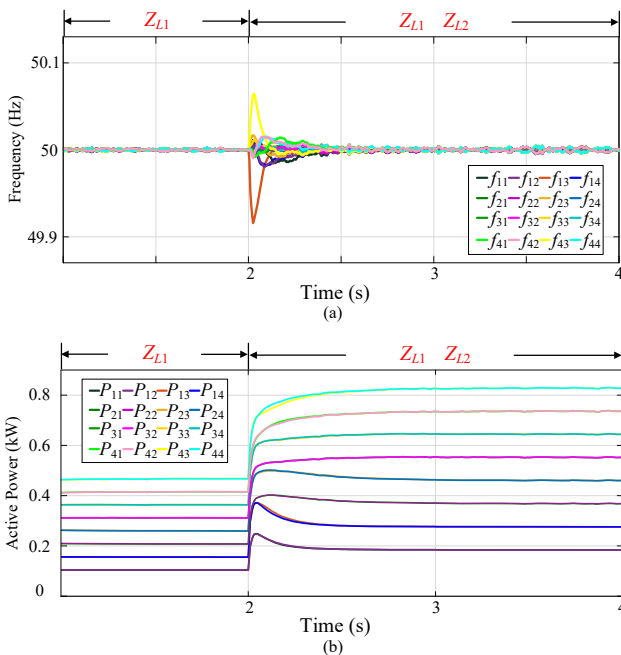


Fig. 15. Simulation results of case I under RL load. (a) Frequency. (b) Active power. (c) Reactive power.

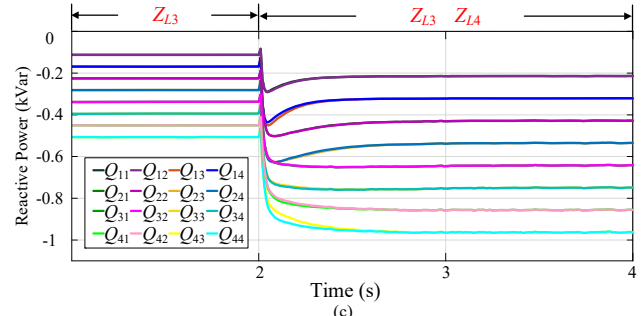
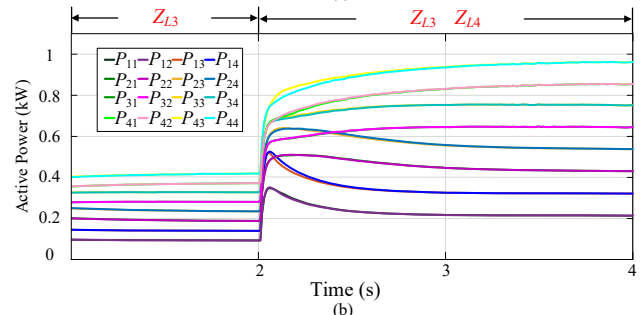
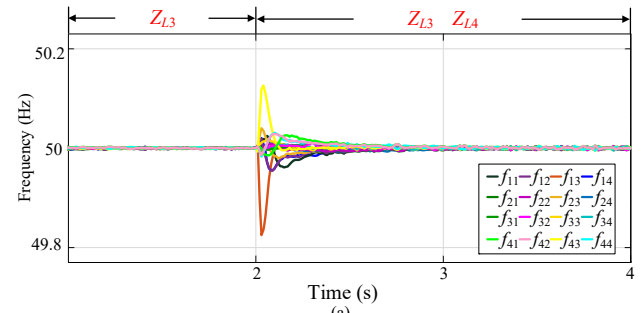


Fig. 16. Simulation results of case I under RC load. (a) Frequency. (b) Active power. (c) Reactive power.

### B. Case II: Performance of Droop Controller

Performance of conventional droop controller is tested in this case, where conventional droop controller is enabled during 2-5s and the proposed unified distributed controller is activated during 0-2s and 5-8s. Fig. 17-18 show frequency responses of DGs under RL load and RC load. It can be seen that hybrid cascaded-parallel microgrid with RL and RC load would become unstable once droop controller is activated, which agrees with theoretical analysis in Section II. Compared with droop control strategy, the proposed distributed control strategy can ensure the system stability without frequency deviation under both RL and RC load.

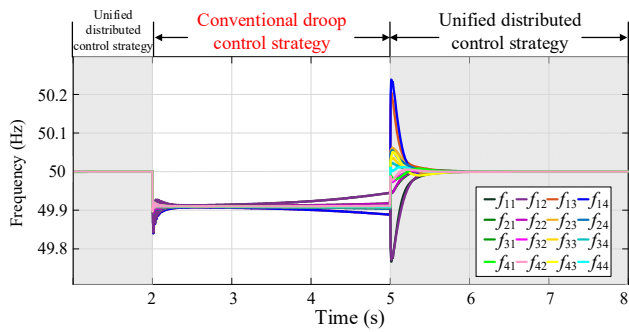


Fig. 17. Simulation result of case II under RL load.

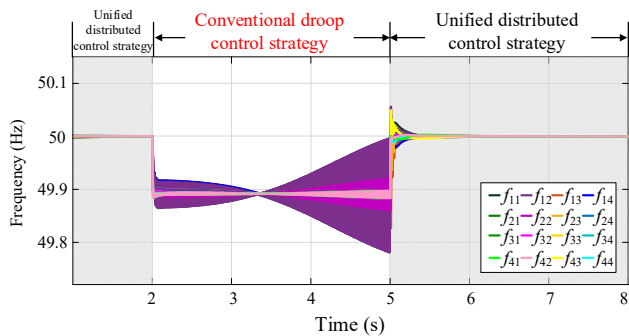


Fig. 18. Simulation result of case II under RC load.

### C. Case III: Communication Delay

To investigate the effect of communication delay on system stability, controller performance with different delay time ( $\tau=50\text{ms}$  and  $\tau=100\text{ms}$ ) is presented in Fig. 19 and Fig. 20. Controller performances under RC load are omitted since they are similar with those under RL load. Load change is same as it in case I. Fig. 19 shows the system frequency with  $\tau=50\text{ms}$ . It can be seen that frequency synchronization is achieved at steady state and only little fluctuations are caused during transients. The active and reactive power results are omitted since they are similar with those in case I. In Fig. 20, bigger fluctuations and even the system oscillation during steady state are triggered when  $\tau=100\text{ms}$ . From Fig. 19 and Fig. 20, it can be seen that communication delay may mitigate system stability if delay time is higher than critical value of stability region. Here, the proposed controller has a good immunity capability for communication system within delay time 50ms, which ensures system stability for existing communication protocols including WiFi and ultrawideband (UWB) [27].

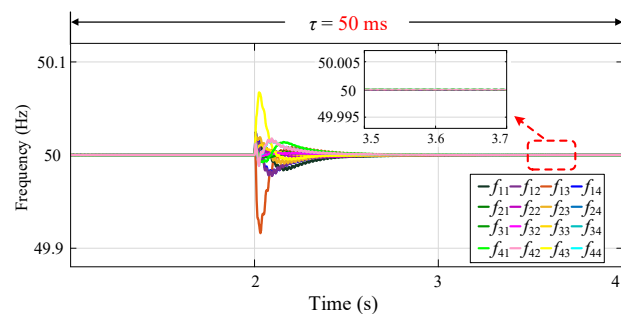


Fig. 19. Simulation result as  $\tau=50\text{ms}$ .

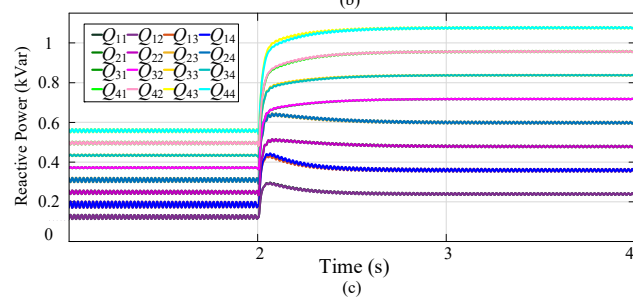
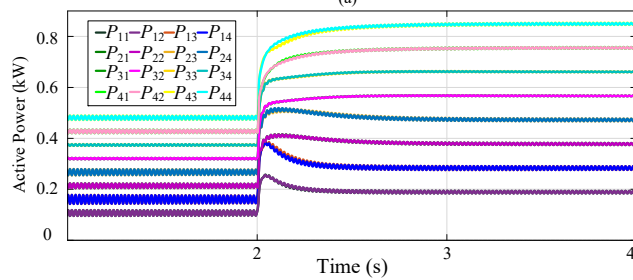
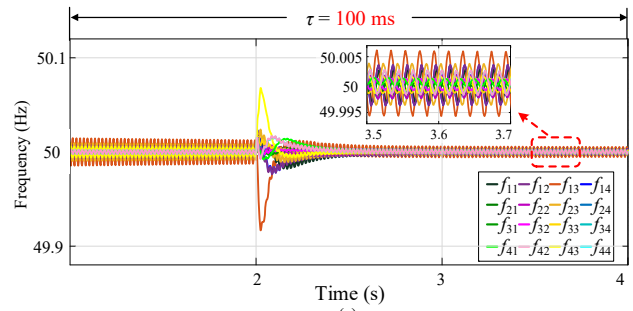


Fig. 20. Simulation results as  $\tau=100\text{ms}$ . (a) Frequency. (b) Active power. (c) Reactive power.

### D. Case IV: Communication Link Failure

In this case, resiliency to the communication link failure is investigated. To test controller performance under cyber network with the minimum connectivity, links 13-14, 23-24, 33-34, 43-44 and 14-24 fail at 0.25s, which is illustrated in Fig. 21. It can be seen from Fig. 21 that the system remains connected under the new graph. Therefore, the link failure should have no effect on the steady-state performance. In order to test the response to load change, load  $Z_{L2}$  is attached and detached at 0.5s and 2.5s respectively. The performance of controller is identical under RL load and RC load, and thus we omit the plots under RC load due to space consideration. Fig. 22 shows frequency and power distribution results under communication link failure. It can be seen that communication link failure does not affect the steady-state performance while it slows down the system dynamics.

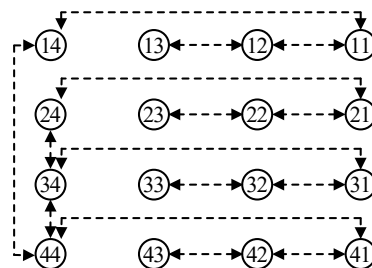


Fig. 21. Cyber configuration in case IV.

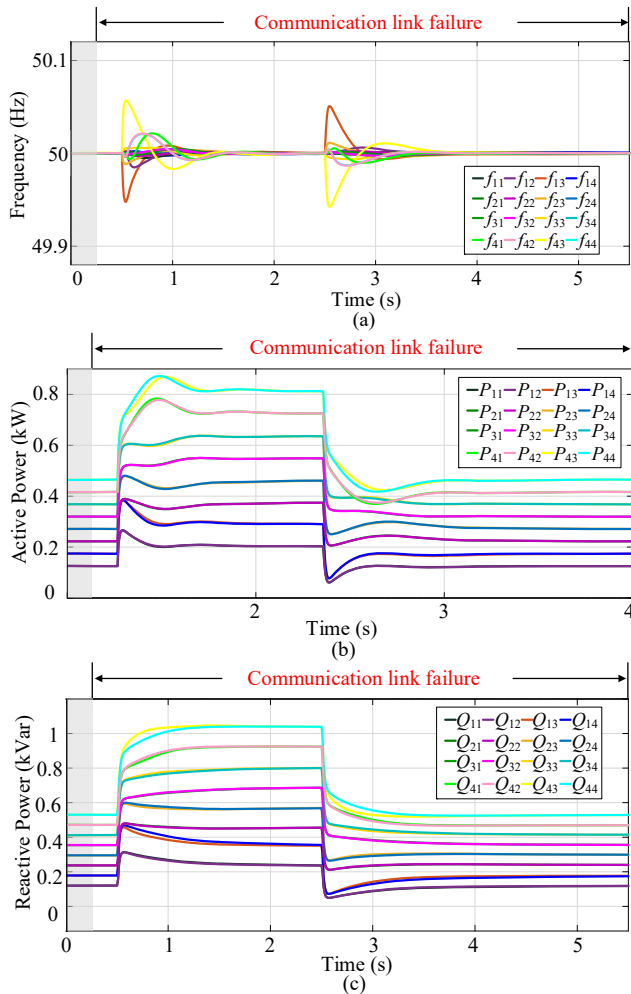


Fig. 22. Simulation results of case IV. (a) Frequency. (b) Active power. (c) Reactive power.

### E. Case V: Plug-and-Play Characteristic

Plug-and-play characteristic of the proposed distributed control method is tested, via unplugging the String#4 at 0.5s and plugging it back in at 2.5s. The two physical configurations are illustrated in Fig. 23 and simulation results are displayed in Fig. 24. It should be noted that when String#4 is unplugged, the communication link 34-44 is disabled at the same time. Nevertheless, the cyber network remains connected and, thus, the steady-state performance is not compromised. From Fig. 24, the power supplied by String#4 reduces to zero during 0.5s~2.5s and the excess power is proportionately shared among remaining DGs. After String#4 is reconnected at 2.5s, the controllers successfully respond to the inverter plugging and share load demand among all DGs.

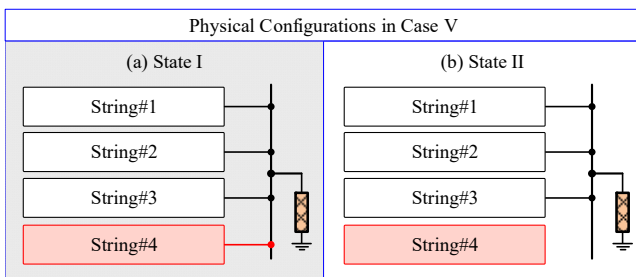


Fig. 23. Physical configuration in case V.

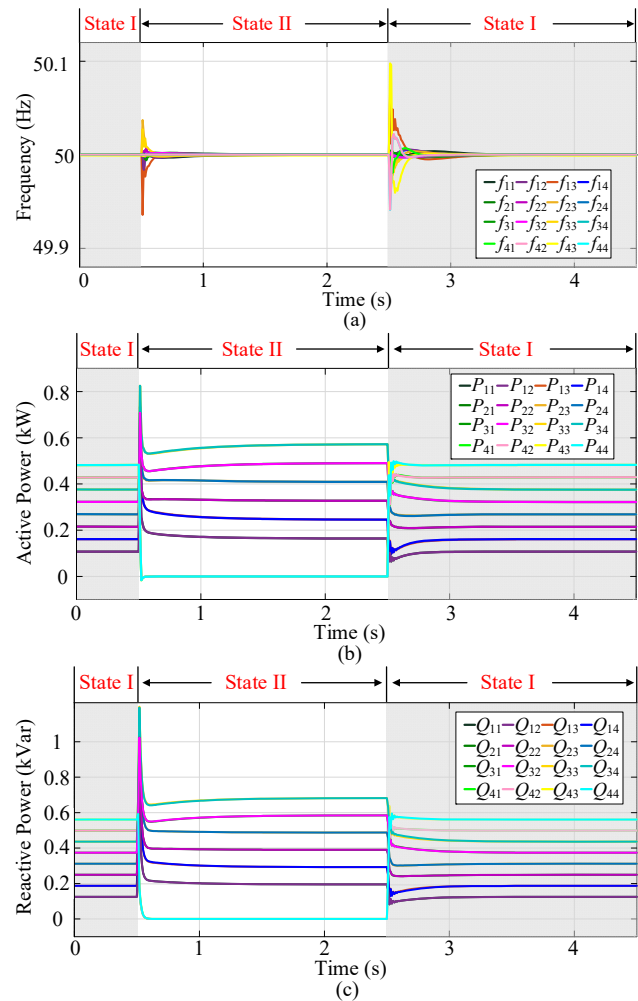


Fig. 24. Simulation results of case V. (a) Frequency. (b) Active power. (c) Reactive power.

## VI. CONCLUSIONS

This paper presents a unified distributed control strategy for hybrid cascaded-parallel microgrid with different load types, where active power and reactive power regulators without frequency drop are developed. A low bandwidth communication network is designed to support power control and improve system redundancy. Furthermore, small signal model of hybrid cascaded-parallel microgrid is established. And small signal stability and dynamic performance is investigated. Eigenvalue analysis shows that parameters of active power regulator and reactive power regulator have critical influences on system stability and dynamic performance. Simulation results show that the unified distributed control strategy is able to implement desirable power sharing under RL load and RC load with superior control performance. Also, the steady-state performance of proposed control strategy is slightly affected in the presence of communication delay and communication link failure. In addition, the distributed control strategy is able to improve system redundancy and support plug-and-play operation of microgrid.

## APPENDIX

The variable vectors ( $\Delta P^{pu}$ ,  $\Delta Q^{pu}$ ,  $\Delta \tilde{\delta}$  and  $\Delta V$ ) and parameter matrixes ( $K_{p^{pu}\tilde{\delta}}$ ,  $K_{p^{pu}V}$ ,  $K_{q^{pu}\tilde{\delta}}$  and  $K_{q^{pu}V}$ ) in (21) are given as (25)-(26).

$$\begin{cases} \Delta P^{pu} = [\Delta P_{11}^{pu} \Delta P_{12}^{pu} \dots \Delta P_{nm_n}^{pu}]^T, & \Delta Q^{pu} = [\Delta Q_{11}^{pu} \Delta Q_{12}^{pu} \dots \Delta Q_{nm_n}^{pu}]^T \\ \Delta \tilde{\delta} = [\Delta \tilde{\delta}_{11} \Delta \tilde{\delta}_{nm_n} \dots \Delta \tilde{\delta}_{nm_n}]^T, & \Delta V = [\Delta V_{11} \Delta V_{12} \dots \Delta V_{nm_n}]^T \\ K_{p^{pu}\tilde{\delta}} = \begin{bmatrix} k_{p_{11}^{pu}\tilde{\delta}_{11}} & k_{p_{11}^{pu}\tilde{\delta}_{12}} & \dots & k_{p_{11}^{pu}\tilde{\delta}_{nm_n}} \\ k_{p_{12}^{pu}\tilde{\delta}_{11}} & k_{p_{12}^{pu}\tilde{\delta}_{12}} & \dots & k_{p_{12}^{pu}\tilde{\delta}_{nm_n}} \\ \vdots & \vdots & \ddots & \vdots \\ k_{p_{nm_n}^{pu}\tilde{\delta}_{11}} & k_{p_{nm_n}^{pu}\tilde{\delta}_{12}} & \dots & k_{p_{nm_n}^{pu}\tilde{\delta}_{nm_n}} \end{bmatrix}, & K_{p^{pu}V} = \begin{bmatrix} k_{p_{11}^{pu}V_{11}} & k_{p_{11}^{pu}V_{12}} & \dots & k_{p_{11}^{pu}V_{nm_n}} \\ k_{p_{12}^{pu}V_{11}} & k_{p_{12}^{pu}V_{12}} & \dots & k_{p_{12}^{pu}V_{nm_n}} \\ \vdots & \vdots & \ddots & \vdots \\ k_{p_{nm_n}^{pu}V_{11}} & k_{p_{nm_n}^{pu}V_{12}} & \dots & k_{p_{nm_n}^{pu}V_{nm_n}} \end{bmatrix} \\ K_{q^{pu}\tilde{\delta}} = \begin{bmatrix} k_{q_{11}^{pu}\tilde{\delta}_{11}} & k_{q_{11}^{pu}\tilde{\delta}_{12}} & \dots & k_{q_{11}^{pu}\tilde{\delta}_{nm_n}} \\ k_{q_{12}^{pu}\tilde{\delta}_{11}} & k_{q_{12}^{pu}\tilde{\delta}_{12}} & \dots & k_{q_{12}^{pu}\tilde{\delta}_{nm_n}} \\ \vdots & \vdots & \ddots & \vdots \\ k_{q_{nm_n}^{pu}\tilde{\delta}_{11}} & k_{q_{nm_n}^{pu}\tilde{\delta}_{12}} & \dots & k_{q_{nm_n}^{pu}\tilde{\delta}_{nm_n}} \end{bmatrix}, & K_{q^{pu}V} = \begin{bmatrix} k_{q_{11}^{pu}V_{11}} & k_{q_{11}^{pu}V_{12}} & \dots & k_{q_{11}^{pu}V_{nm_n}} \\ k_{q_{12}^{pu}V_{11}} & k_{q_{12}^{pu}V_{12}} & \dots & k_{q_{12}^{pu}V_{nm_n}} \\ \vdots & \vdots & \ddots & \vdots \\ k_{q_{nm_n}^{pu}V_{11}} & k_{q_{nm_n}^{pu}V_{12}} & \dots & k_{q_{nm_n}^{pu}V_{nm_n}} \end{bmatrix} \end{cases} \quad (25)$$

where

$$\begin{cases} k_{p_{ij}^{pu}\tilde{\delta}_{ab}} = \frac{\partial p_{ij}^{pu}}{\partial \tilde{\delta}_{ab}}, & k_{p_{ij}^{pu}V_{ab}} = \frac{\partial p_{ij}^{pu}}{\partial V_{ab}} \\ k_{q_{ij}^{pu}\tilde{\delta}_{ab}} = \frac{\partial q_{ij}^{pu}}{\partial \tilde{\delta}_{ab}}, & k_{q_{ij}^{pu}V_{ab}} = \frac{\partial q_{ij}^{pu}}{\partial V_{ab}} \end{cases} \quad \left( \begin{matrix} i=1, \dots, n & j=1, \dots, m_i \\ a=1, \dots, n & b=1, \dots, m_a \end{matrix} \right) \quad (26)$$

The control coefficient matrixes ( $K_\omega$ ,  $K_{\omega_p}$ ,  $K_p$ ,  $K_I$ ,  $K_{p_p}$  and  $K_{I_p}$ ) and Laplacian matrixes ( $L_s$  and  $L_p$ ) in (22) are given as (27).

$$\begin{cases} K_\omega = \text{diag}\{k_\omega^{ij}\}, & K_{\omega_p} = \text{diag}\{k_{\omega_p}^{ij}\}, & K_p = \text{diag}\{k_p^{ij}\} \\ K_I = \text{diag}\{k_I^{ij}\}, & K_{p_p} = \text{diag}\{k_{p_p}^{ij}\}, & K_{I_p} = \text{diag}\{k_{I_p}^{ij}\} \\ A_{I_s} = \begin{bmatrix} 0 & a_{i1\_i2} & \dots & a_{i1\_im_i} \\ a_{i2\_i1} & 0 & \dots & a_{i2\_im_i} \\ \vdots & \vdots & \ddots & \vdots \\ a_{im_i\_i1} & a_{im_i\_i2} & \dots & 0 \end{bmatrix} \\ D_{I_s}^{in} = \text{diag}\{d_{ij\_s}^{in}\}, & d_{ij\_s}^{in} = \sum_h a_{ij\_h} \\ L_s = \text{diag}\{L_{I_s}\}, & L_{I_s} = D_{I_s}^{in} - A_{I_s} \\ A_{I\_k\_p} = \begin{bmatrix} a_{i1\_j1} & a_{i1\_j2} & \dots & a_{i1\_jm_j} \\ a_{i2\_j1} & a_{i2\_j2} & \dots & a_{i2\_jm_j} \\ \vdots & \vdots & \ddots & \vdots \\ a_{im_i\_j1} & a_{im_i\_j2} & \dots & a_{im_i\_jm_j} \end{bmatrix} \\ A_p = \begin{bmatrix} 0_{m_1 \times m_1} & A_{1\_2\_p} & \dots & A_{1\_n\_p} \\ A_{2\_1\_p} & 0_{m_2 \times m_2} & \dots & A_{2\_n\_p} \\ \vdots & \vdots & \ddots & \vdots \\ A_{n\_1\_p} & A_{n\_2\_p} & \dots & 0_{m_n \times m_n} \end{bmatrix} \\ D_{I\_p}^{in} = \text{diag}\{d_{ij\_p}^{in}\}, & d_{ij\_p}^{in} = \sum_r a_{ij\_r}, & L_p = A_p - \text{diag}\{D_{I\_p}^{in}\} \end{cases} \quad \left( \begin{matrix} i=1, 2, \dots, n \\ l=1, 2, \dots, n \\ j=1, 2, \dots, m_n \\ h \in N_{ij\_s} \\ r \in N_{ij\_p} \end{matrix} \right) \quad (27)$$

## REFERENCES

- [1] R. H. Lasseter, "Smart distribution: Coupled microgrids," *Proc. IEEE*, vol. 99, no. 6, pp. 1074–1082, Jun. 2011.
- [2] M. S. G. Esfahani, Q. Shafiee, D. D.-C. Lu, and J. M. Guerrero, "Distributed control of low-voltage resistive AC microgrids," *IEEE Trans. Energy Convers.*, vol. 34, no. 2, pp. 573–584, Jun. 2019.
- [3] Y. Wang, Z. Chen, X. Wang, Y. Tian, Y. Tan, and C. Yang, "An estimator-based distributed voltage predictive control strategy for AC islanded microgrids," *IEEE Trans. Power Electron.*, vol. 30, no. 7, pp. 3934–3951, Jul. 2015.
- [4] X. Hou, Y. Sun, X. Zhang, G. Zhang, J. Lu, and F. Blaabjerg, "A self-synchronized decentralized control for series-connected H-bridge rectifiers," *IEEE Trans. Power. Electron.*, vol. 34, no. 8, pp. 7136–7142, Aug. 2019.
- [5] J. He, Y. W. Li, C. Wang, Y. Pan, C. Zhang, and X. Xing, "A hybrid microgrid with parallel and series connected micro-converters," *IEEE Trans. Power Electron.*, vol. 33, no. 6, pp. 4817–4831, Jun. 2018.
- [6] X. Ge, H. Han, W. Yuan, Y. Sun, M. Su, and K. L. Hai, "An integrated series-parallel microgrid structure and its unified distributed control," in *Proc. IEEE SPEC*, 2018, pp. 1–6.
- [7] Y. Wang, D. Liu, P. Liu, F. Deng, D. Zhou, and Z. Chen, "Lifetime-oriented droop control strategy for AC islanded microgrids," *IEEE Trans. Ind. Appl.*, vol. 55, no. 3, pp. 3252–3263, May/Jun. 2019.
- [8] Y. Wang, X. Wang, Z. Chen, and F. Blaabjerg, "Small-signal stability analysis of inverter-fed power systems using component connection method," *IEEE Trans. Smart Grid*, vol. 9, no. 5, pp. 5301–5310, Sep. 2018.
- [9] H. Han, X. Hou, J. Yang, J. Wu, M. Su, and J. M. Guerrero, "Review of power sharing control strategies for islanding operation of AC microgrids," *IEEE Trans. Smart Grid*, vol. 7, no. 1, pp. 200–215, Jan. 2016.
- [10] A. G. Tsikalakis and N. D. Hatziargyriou, "Centralized control for optimizing microgrids operation," *IEEE Trans. Energy Convers.*, vol. 23, no. 1, pp. 241–248, Mar. 2008.
- [11] M. M. A. Abdelaziz, M. F. Shaaban, H. E. Farag, and E. F. El-Saadany, "A multistage centralized control scheme for islanded microgrids with PEV," *IEEE Trans. Sustain. Energy*, vol. 5, no. 3, pp. 927–937, Jul. 2014.
- [12] J. Yang, W. Yuan, Y. Sun, H. Han, X. Hou, and J. M. Guerrero, "A novel quasi-master-slave control frame for PV-storage independent microgrid," *International Journal of Electrical Power and Energy Systems*, vol. 97, pp. 262–274, Apr. 2018.
- [13] N. M. Dehkordi, N. Sadati, and M. Hamzeh, "Fully distributed cooperative secondary frequency and voltage control of islanded microgrids," *IEEE Trans. Energy Convers.*, vol. 32, no. 2, pp. 675–685, Jun. 2017.
- [14] Y. Wang, X. Wang, Z. Chen, and F. Blaabjerg, "Distributed optimal control of reactive power and voltage in islanded microgrids," *IEEE Trans. Ind. Appl.*, vol. 53, no. 1, pp. 340–349, Jan./Feb. 2017.
- [15] J. Hu, J. Duan, H. Ma, and M. Y. Chow, "Distributed adaptive droop control for optimal power dispatch in DC microgrid," *IEEE Trans. Ind. Electron.*, vol. 65, no. 1, pp. 778–789, 2018.
- [16] Z. Liu, M. Su, Y. Sun, H. Han, X. Hou, and J. M. Guerrero, "Stability analysis of DC microgrids with constant power load under distributed control methods," *Automatica*, vol. 90, pp. 62–72, Apr. 2018.
- [17] Y. Wang, X. Wang, F. Blaabjerg, and Z. Chen, "Harmonic instability assessment using state-space modeling and participation analysis in inverter-fed power system," *IEEE Trans. Ind. Electron.*, vol. 64, no. 1, pp. 806–816, Jan. 2017.
- [18] M. Patterson, N. F. Macia, and A. M. Kannan, "Hybrid microgrid model based on solar photovoltaic battery fuel cell system for intermittent load applications," *IEEE Trans. Energy Convers.*, vol. 30, no. 1, pp. 359–366, Sep. 2014.
- [19] E. Chatzinikolaou and D. J. Rogers, "A comparison of grid-connected battery energy storage system designs," *IEEE Trans. Power Electron.*, vol. 32, no. 9, pp. 6913–6923, Sep. 2017.
- [20] M. Malinowski, K. Gopakumar, J. Rodriguez, and M. P. Perez, "A survey on cascaded multilevel inverters," *IEEE Trans. Ind. Electron.*, vol. 57, no. 7, pp. 2197–2206, Jul. 2010.
- [21] L. Maharjan, S. Inoue, H. Akagi, and J. Asakura, "State-of-charge (SOC)-balancing control of a battery energy storage system based on a cascade PWM converter," *IEEE Trans. Power Electron.*, vol. 24, no. 6, pp. 1628–1636, Jun. 2009.
- [22] J. He, Y. Li, B. Liang, and C. Wang, "Inverse power factor droop control for decentralized power sharing in series-connected micro-converters

based islanding microgrids," *IEEE Trans. Ind. Electron.*, vol. 64, no. 9, pp. 7444-7454, Sep. 2017.

- [23] Y. Sun, G. Shi, X. Li, W. Yuan, M. Su, H. Han, and X. Hou, "An f-P/Q droop control in cascaded-type microgrid," *IEEE Trans. Power Systems*, vol. 33, no. 1, pp. 1136-1138, Jan. 2018.
- [24] W. Yuan, J. Yang, G. Shi, Y. Sun, H. Han, and X. Hou, "Control design and stability analysis for the cascaded-type AC microgrid," in *Proc. IEEE IECON*, 2017, pp. 2407-2412.
- [25] X. Hou, Y. Sun, H. Han, Z. Liu, W. Yuan, and M. Su, "A fully decentralized control of grid-connected cascaded inverters," *IEEE Trans. Sustainable Energy*, vol.10, no.1, pp. 315-317, Jan. 2019.
- [26] M. C. Chandorkar, D. M. Divan, and R. Adapa, "Control of parallel connected inverters in standalone ac supply systems," *IEEE Trans. Ind. Appl.*, vol.29, no.1 pp.136-143, Jan.1993.
- [27] V. Nasirian, Q. Shafiee, J. M. Guerrero, F. L. Lewis, and A. Davoudi, "Droop-free distributed control for AC microgrids," *IEEE Trans. Power Electron.*, vol. 31, no.2, pp.1600-1617, Feb. 2016.
- [28] A. Bidram, A. Davoudi, F. L. Lewis, and S. S. Ge, "Distributed adaptive voltage control of inverter-based microgrids," *IEEE Trans. Energy Convers.*, vol. 29, no. 4, pp. 862-872, Dec. 2014.
- [29] E. A. A. Coelho, P. C. Cortizo, and P. F. D. Garcia, "Small-signal stability for parallel-connected inverters in stand-alone AC supply systems," *IEEE Trans. Ind. Appl.*, vol. 38, no. 2, pp. 533-542, Mar/Apr. 2002.
- [30] J. W. Simpson-Porco, F. Dörfler, and F. Bullo, "Synchronization and power sharing for droop-controlled inverters in islanded microgrids," *Automatica*, vol. 49, no. 9, pp. 2603-2611, 2012.
- [31] Z. Liu, M. Su, Y. Sun, W. Yuan, H. Han, and J. Feng, "Existence and stability of equilibrium of DC microgrid with constant power loads," *IEEE Trans. Power Systems*, vol. 33, no. 6, pp. 6999-7010, Nov. 2018.



**Wenbin Yuan** received the B.E. degree from Xiangtan University, Xiangtan, China, in 2015, and M.S. degree from the School of Information Science and Engineering, Central South University, Changsha, China, in 2018.

Currently, he is working toward Ph.D. degree in the department of Energy Technology, Aalborg University, Denmark.

His research interests include distributed power generation system, microgrid, as well as control technologies of power electronic-dominated power system.



**Yanbo Wang** (S'15-M'17) received Ph.D. degree in the department of Energy Technology, Aalborg University, Denmark in 2017.

Currently, he is with the department of Energy Technology in Aalborg University as a Postdoctoral Fellow. From June to October of 2016, he was a visiting scholar in Power System Research Group of the

Department of Electrical and Computer Engineering, University of Manitoba, Winnipeg, MB, Canada. His research interests include distributed power generation system, wind

power system, microgrid, as well as operation and control technologies of power electronic-dominated power system.

Dr. Wang's paper on Distributed Power System received the First Prize Paper Award of the 6th International Conference of Smart Grid cosponsored by IEEE Industry Application Society in 2017. He received the Best Session Paper Award at the annual conference of the IEEE Industrial Electronics Society in 2015 in Japan.



**Xiaohai Ge** was born in Anhui, China, in 1996. He received the B.S. degree from the School of Information Science and Engineering, Central South University, Changsha, China, in 2017, where he is currently working toward M.S. degree in Electrical Engineering.

His research interests include renewable energy systems, distributed micro-grid, and power-electronic enabled

power network.



**Xiaochao Hou** received the B.S. and M.S. degrees from the School of Information Science and Engineering, Central South University, Changsha, China, in 2014 and 2017, respectively, where he is currently working toward Ph.D. degree in power electronics and power transmission.

Now he is a joint Ph.D. student supported by the China Scholarship Council with the School of Electrical and

Electronic Engineering of Nanyang Technological University. His research interests include renewable energy systems, distributed micro-grid, and power-electronic enabled power network.



**Hua Han** was born in Hunan, China, in 1970. She received the M.S. and Ph.D. degrees from the School of Automation, Central South University, Changsha, China, in 1998 and 2008, respectively. She was a Visiting Scholar with the University of Central Florida, Orlando, FL, USA, from 2011 to 2012. She is currently a Professor with the School of Automation,

Central South University.

Her research interests include microgrids, renewable energy power generation systems, and power electronic equipment.